Use of Fluorescence Resonance Energy Transfer To Investigate the Conformation of DNA Substrates Bound to the Klenow Fragment†

W. Scott Furey,‡ Catherine M. Joyce,§ Mark A. Osborne,‡ David Klenerman,‡ James A. Peliska,⊥ and Shankar Balasubramanian*,‡

University Chemical Laboratory, Cambridge University, Lensfield Road, Cambridge CB2 1EW, U.K., Department of Molecular Biophysics and Biochemistry, Yale University, New Haven, Connecticut 06520-8114, and Department of Biological Chemistry, University of Michigan Medical School, Ann Arbor, Michigan 48109

Received August 11, 1997; Revised Manuscript Received November 11, 1997

ABSTRACT: Fluorescence resonance energy transfer (FRET) has been used to investigate the conformation of the single stranded region for a series of fluorescent DNA template−primers bound to the Klenow fragment (KF) of *Escherichia coli* DNA polymerase I. Fluorescent derivatives of template−primer DNA, modified with tetramethylrhodamine (TMR), served as energy transfer acceptors to the donor fluorescein fluorophore used to modify cysteine 751 in the double mutant KF (S751C, C907S). Design of the template−primer allowed the probe's position within the DNA−protein complex to be varied by stepwise extension of the primer strand upon addition of the appropriate deoxynucleoside triphosphates (dNTP). The TMR acceptor probe occupied seven different positions in the template−primers, five in the single stranded region and two in the double stranded region. The efficiency of energy transfer was determined at each position by calculating the integrated area of the fluorescein emission peak in the presence and absence of acceptor. Results indicate that the FRET efficiency varied in a sinusoidal fashion with a periodicity of approximately 10 base pairs and that the data could be fitted to an equation derived from a simple model formulated on the basis of helical structure. The data support the conclusion that the single stranded template portion of a DNA template−primer adopts a helical conformation when bound to the KF. The results of this study further support FRET as a useful method for the determination of structure and conformation in protein−DNA complexes.

Escherichia coli DNA polymerase I (Pol I)[1] is a multifunctional enzyme responsible for DNA repair and replication in vivo (*1*). In addition to the 5′−3′ polymerase activity of the enzyme, the separate 3′−5′ and 5′−3′ exonuclease activities are all found on a single 103 kDa polypeptide chain. The large 68 kDa proteolytic fragment of Pol I, termed the Klenow fragment, retains the polymerase and 3′−5′ exonuclease activities. The Klenow fragment has served as a prototype system for more complex polymerases. Since the original crystal structure was obtained (*2*), the Klenow fragment has been studied intensely by a variety of structural (e.g. 3−5), kinetic (e.g. refs 6−8), genetic (e.g. refs 9−12), and spectroscopic (e.g. 13 and 14) techniques in order to gain insight into polymerase mechanisms and DNA−protein interactions in such systems.

There has recently been a significant improvement in our knowledge of the structures of template-directed polynucleotide polymerases and their interactions with nucleic acid substrates. Crystal structures of seven nucleic acid polymerases are now available: the Klenow fragment of *E. coli* DNA polymerase I (KF) (*2*−*5*), HIV-1 reverse transcriptase (RT) (*15*−*17*), Moloney murine leukemia virus reverse transcriptase (*18*), bacteriophage T7 RNA polymerase (*19*), rat DNA polymerase β (*20, 21*), Taq polymerase (*22*−*24*), and a thermostable *Bacillus* DNA polymerase I (*25*). The most recent crystal structure of Taq polymerase complexed with duplex DNA (*22*) supports the conclusions of Steitz and co-workers (*3*) and would appear to have resolved the debate regarding the orientation of DNA binding (*26*−*28*). On the basis of the structural homology between Taq polymerase and the KF, it would appear reasonable to assume that the KF binds the duplex region in the same manner. Some of these structural studies have involved polymerase−nucleic acid cocrystal structures (*3, 5, 15, 17, 21, 22*) and have addressed the issue of polymerase−nucleic acid interactions. One issue which has not been addressed in detail

† S.B. is a Royal Society Research Fellow. This work was supported by an NSERC 1967 fellowship to W.S.F. and NIH Grant GM-28550 to C.M.J.

* To whom correspondence should be addressed at the Cambridge University. Phone: +44-1223-336347. Fax: +44-1223-336913. E-mail: sb10031@cam.ac.uk.

‡ Cambridge University.

§ Yale University.

⊥ University of Michigan.

[1] Abbreviations: Pol I, *Escherichia coli* DNA polymerase I; KF, Klenow fragment; KF*, fluorescein modified Klenow fragment; TMR, tetramethylrhodamine; dNTP, deoxynucleoside 5′-triphosphate; bp, base pair; kDa, kilodalton; Da, dalton; FRET, fluorescence resonance energy transfer; ESMS, electrospray mass spectrometry; HPLC, high-pressure liquid chromatography; fwhm, full width at half-maximum; TEAB, triethylammonium bicarbonate; TEA, triethylamine; EDTA, ethylenediaminetetraacetic acid; DTT, dithiothreitol; DMF, dimethylformamide; IPA, 2-propanol; Tris-HCl, tris(hydroxymethyl)aminomethane hydrochloride; KP_i, potassium dihydrogen phosphate/dipotassium hydrogen phosphate; RT, reverse transcriptase; 35*, a TMR labeled 35 mer template oligonucleotide (see Figure 1); 38*, a TMR labeled 38 mer template oligonucleotide (see Figure 1).

S0006-2960(97)01975-2 CCC: $15.00
Published on Web 02/10/1998

is the structure and conformation of the single stranded template region situated beyond the primer terminus. Any ordered structure, or lack thereof, in this region could be of significance in understanding the molecular basis of polymerase fidelity mechanisms, specifically with regard to the sequence of events that occurs during DNA melting and translocation from the polymerase to exonuclease active sites. Previous work by Benkovic and co-workers used fluorescent oligonucleotide duplexes to elucidate points of strong enzyme−DNA contacts in complexes of KF with various template−primer systems (*29*). Modulations in fluorescence intensity and anisotropy measurements have suggested the possibility that the single stranded template region may adopt a helical conformation when bound to the enzyme (*29*). No crystal structure has yet shown a competent complex with bound duplex DNA at the polymerase active site and an extended template region as cocrystals of such structures have proven difficult to obtain (*4*). Therefore, other methods more amenable to such studies must be employed in order to advance the structural understanding of DNA−polymerase complexes.

One such method which has found wide use in biochemistry and structural biology applications is fluorescence resonance energy transfer (FRET) (*30*−*32*). In FRET, energy is transferred nonradiatively from a donor molecule to an acceptor molecule via an induced dipole interaction with the transfer efficiency, *E*, depending on the inverse-sixth-power of the distance *R* between the donor and acceptor: $E = \{1/(1 + [R/R_0]^6)\}$. Owing to its utility for measuring interactions in the range of 10−100 Å and for its sensitivity to small changes in distance between fluorophores, FRET has been used extensively to investigate macromolecular assemblies in biological systems. Examples include molecular interactions in proteins (*33*) and distance measurements between substrate binding sites in protein−DNA complexes (*34*). Specific applications to structural studies of DNA include the study of the helical geometry of duplex DNA in solution (*35*) and the investigation of oligonucleotide interactions such as duplex hybridization (*36*) and triple helix formation (*37*). In this paper we report the use of FRET to investigate the structure and conformation of the single stranded template region of a template−primer DNA substrate when bound to the KF. The data support the conclusions that the single stranded region is ordered and appears to adopt a helical conformation with structural parameters generated from a simple vector model of the DNA−polymerase interaction.

EXPERIMENTAL PROCEDURES

Materials. 5-Carboxytetramethylrhodamine (and 6-carboxytetramethylrhodamine) and iodoacetamidofluorescein were purchased from Molecular Probes. γ-^{32}P[ATP] was from DuPont NEN. Nucleotide triphosphates, NAP-10, and PD-10 columns were from Pharmacia. Centricon-30 concentrators were from Amicon. All other reagents were of the highest quality commercially available. Oligonucleotides were purchased from OSWEL DNA Service (Southampton). Concentration under vacuum of solutions of oligonucleotides and other low-volume solutions was performed using a GeneVac SF50 centrifugal evaporator with CVP100 pump.

Construction and Purification of the Mutant Klenow Fragment Derivative. The mutation C907S, which removes the unique cysteine of the KF, and S751C, which introduces a novel cysteine substitution, were constructed and subcloned into an overproducer plasmid following previously published procedures (*11*). The S751C, C907S double mutant protein was expressed by heat induction in the host strain CJ376 (*38*) and purified as described (*39*). The protein was stored at −20 °C in a buffer of 50 mM Tris-HCl, pH 7.5, 1 mm DTT, containing 50% glyerol. The glycerol was removed by dialysis prior to conjugation with fluorescent dyes. Protein concentrations were determined spectroscopically using $\epsilon_{278} = 6.32 \times 10^4$ M^{-1} cm^{-1} (*40*).

Sulfhydryl Modification of the Klenow Fragment. Protein samples stored in 50% glycerol were dialyzed against 50 mM Tris-HCl, pH 7.5, containing 1 mM DTT. The Klenow fragment (2.5 mL, 20 μM) was loaded onto a PD-10 column (equilibrated with argon purged 0.1 N KP_i, pH 7.5) and eluted in 1 mL fractions. Fractions containing protein were located by A_{280}, pooled, and concentrated to 120 μM (200 μL) using a Centricon-30 concentrator. A 200 mM solution iodoacetamidofluorescein in DMF (0.5 μL) was added to the protein solution to give a final concentration of 360 μM. The reaction proceeded for 30 min at 4 °C. The reaction was quenched by addition of DTT to 5 mM, purified by passage through a PD-10 column equilibrated in 50 mM Tris-HCl, pH 7.5, and concentrated as described. The extent of the label incorporated was calculated by UV absorbance at 278 nm, using $\epsilon_{278} = 6.32 \times 10^4$ M^{-1} cm^{-1} for the Klenow fragment, and at 490 nm, using $\epsilon_{490} = 6.8 \times 10^4$ M^{-1} cm^{-1} for fluorescein (*41*). Electrospray mass spectrometry (ESMS) was also used to confirm the extent of label incorporation. The fluorescently modified KF is referred to as KF* in the text.

Single Base Incorporation. To ensure that the polymerase activity of the enzyme was not adversely affected by the fluorescent modification, a single base addition experiment was performed which involved incorporation of dATP into a ^{32}P-labeled 13/20 mer duplex. The sequence of the duplex was

3′-AGCGTCGGCAGGTTCCCAAA-5′

5′-TCGCAGCCGTCCA-3′

5′-^{32}P end labeling of both the template and primer was performed using standard methods (*42*). The single base incorporation was carried out by incubating KF* (0.08 μM) and radiolabeled 13/20 mer (0.4 μM) in a buffer of 50 mM Tris-HCl, pH 7.5, 50 mM NaCl, 0.5 mM EDTA at 25 °C. Polymerization was initiated by addition of a solution of dATP/$MgCl_2$ to give final concentrations of 50 μM and 5.5 mM, respectively. The final volume of the reaction was 100 μL. The 5 μL reaction samples were quenched at 10 s intervals by mixing with a solution of the sequencing gel load buffer containing 0.5 M EDTA. Samples were heated to 90 °C and electrophoresed on a 15% denaturing polyacrylamide sequencing gel. Oligonucleotide products were visualized using a Molecular Dynamics PhosphorImager, and bands were quantitated using the ImageQuant program.

Derivatization of Oligonucleotides. The oligonucleotides used had an amino-modified uridine base (Figure 1) which

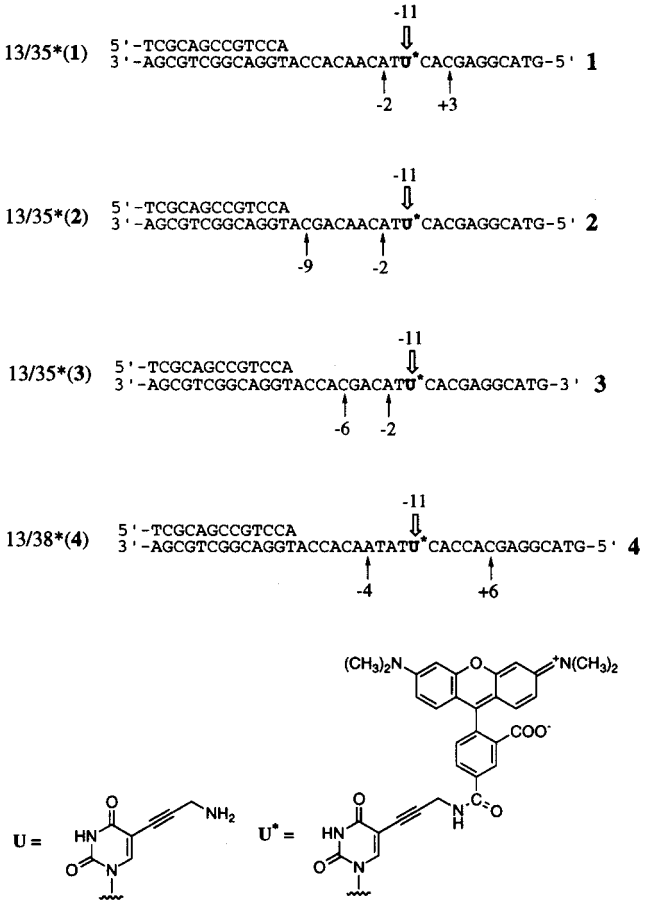

FIGURE 1: Fluorescent template−primer systems. U denotes a derivatizable base, and U*, the TMR-modified conjugate. The primer terminus is defined as position 0, and the relative position of the TMR probe is given a numerical value based on the distance (in bases) from the primer terminus, with bases in the duplex and single stranded regions assigned positive and negative values, respectively. The upper arrow indicates the position (−11) of the TMR fluorophore relative to the primer terminus *prior* to primer strand extension. The lower arrow numbers indicate the position of the TMR probe *following* primer strand extension after the addition of appropriate dNTP's. **1**−**4** refer to the TMR-modified 35* mer or 38* mer template oligonucleotides throughout the text. 13/35*(1), 13/35*(2), 13/35*(3), and 13/38*(4) refer to the duplex substrates containing the indicated template strand. The sequence of the 13 mer primer strand is the same for all four template−primer systems.

was postsynthetically modified by amide bond formation upon reaction with the succinimidyl ester of TMR, using a modified version of a published procedure (*29*).

To 100 nmol template oligonucleotide in 200 mM TEAB, pH 10, was added 4.0 μmol of (21 μL of 190 mM) TMR−succinimidyl ester in DMF to a final concentration of 4 mM. The reaction proceeded for 16 h at room temperature in the dark. The reaction mixture was diluted to 1 mL with water and purified by passage through a NAP-10 column to remove excess fluorescent label. The solution was concentrated under vacuum to 1 mL, purified through a second NAP-10 column, and brought to dryness under vacuum. The TMR-labeled oligonucleotides were further purified by reverse phase HPLC using a Hewlett-Packard 1100 Series HPLC with an attached TosoHaas TSKgel Oligo-DNA RP column (4.6 × 150 mm). One gradient was used for all samples, and all runs were monitored at 254 nm. An attached fluorescence detector allowed TMR fluorescence to be monitored by excitation at 560 nm and measuring emission at 578 nm. Mobile phase A was 0.1 M ammonium acetate, pH 7.0, and mobile phase B was HPLC grade acetonitrile. The gradient was isocratic 5% B for 5 min, 5% B to 30% B in 25 min, isocratic 30% B for 5 min, 30% B to 100% B in 5 min, isocratic 100% B for 3 min, and 100% B to 5% B in 2 min. The flow rate was 1 mL/min. Oligonucleotide concentrations were determined by the absorbance at 260 nm, using extinction coefficients calculated for each oligonucleotide based on the extinction coefficients of each component nucleotide. Values used for each nucleotide were ϵ_{260}(A) = 15 400 M^{-1} cm^{-1}, ϵ_{260}(T) = 8800 M^{-1} cm^{-1}, ϵ_{260}(G) = 11 700 M^{-1} cm^{-1}, ϵ_{260}(C) = 7300 M^{-1} cm^{-1} (*42*).

Formation of Fluorescent Duplexes. The fluorescent duplexes shown in Figure 1 were prepared by mixing the modified 35* or 38* mer template oligonucleotides with a small molar excess (2%) of the 13 mer primer in a buffer of 50 mM Tris-HCl, pH 7.5, 50 mM NaCl. Samples of duplex were annealed by heating to 85 °C for 2 min and slow cooling to 20 °C.

Steady-State Fluorescence Measurements. All fluorescence measurements were performed on a Shimadzu RF-5100 PC spectrofluorometer. The band-pass was 3 nm for the excitation and 5 nm for the emission monochromator. The samples were excited at 497 nm and fluorescence emission spectra collected from 500 to 625 nm using a 10 mm path length microcell (total volume = 50 μL). Measurements were performed in a buffer of 50 mM Tris-HCl, pH 7.5, 0.5 mM EDTA, 100 mM NaCl. All measurements were consistent over four independent experiments using different preparations of protein and DNA samples. The absorbance of solutions used for all fluorescence measurements at the wavelength of excitation was always below 0.015.

Fluorescence Anisotropy Measurements. Anisotropy measurements of both fluorescein-labeled protein and TMR-labeled DNA samples were made at 25 °C on an Aminco-Bowman Series 2 luminescence spectrometer. Fluorescein anisotropy measurements were made on a 1 mL solution containing 5 μM KF* in a buffer of 50 mM Tris-HCl, pH 7.5, 0.5 mM EDTA. Measurements were also performed on samples of KF* with bound nonfluorescent 13/35 mer duplex DNA in a buffer of 50 mM Tris-HCl, pH 7.5, 50 mM NaCl, 0.5 mM EDTA, to obtain anisotropy values for the protein−DNA complex. TMR anisotropy measurements were made in a 1 mL solution containing 5 μM 13/35 mer duplex with the TMR probe positioned in the single stranded and duplex regions, in a buffer of 50 mM Tris, 50 mM NaCl. Measurements were also performed on the same samples bound to nonfluorescent KF protein in the same buffer containing 0.5 mM EDTA in order to obtain bound anisotropy values. Fluorescein and TMR measurements were made with excitation/emission wavelengths of 497/518 and 560/575 nm, respectively. Anisotropy measurements were made with allowance for the grating correction factor (*43*).

Fluorescence Resonance Energy Transfer. On the basis of Förster transfer theory, the efficiency of energy transfer (**E**) is defined as (*44*)

$$E = 1/(1 + [R/R_0])^6) \quad (1)$$

R_0 is the Förster critical distance, where $E = 0.5$ and is

calculated from (*45*)

$$R_0 = (9.79 \times 10^3)(\kappa^2 n^{-4} Q_D J_{DA})^{1/6} \quad (2)$$

where n is the refractive index of the medium, taken to be 1.4 in aqueous solution (*43*), and κ^2 is a geometric factor related to the relative angle of the two transition dipoles, which is assumed to be $^2/_3$ in this study. The overlap integral J_{DA} represents the normalized spectral overlap of the donor emission (F_D) and the acceptor absorption (ϵ_A) according to the equation (*46*)

$$J_{DA} = [\int F_D(\lambda)\, \epsilon_A(\lambda) \lambda^4\, d\lambda]/[\int F_D(\lambda)\, d\lambda] \quad (M^{-1}\, cm^3) \quad (3)$$

J_{DA} was determined by the numeric integration of the normalized emission spectra of KF* bound to a nonfluorescent 13/35 mer duplex and the absorption spectra of a 13/35 mer duplex labeled with TMR in the single stranded region (at position −11) and bound to nonfluorescent KF protein. Integration was performed between 400 and 650 nm. Q_D, the quantum yield of the donor in the absence of acceptor, was calculated using (*47*)

$$Q_D = Q_{RF}(I_D/I_{RF})(A_{RF}/A_D) \quad (4)$$

where I_D and I_{RF} are the respective fluorescence intensities of the donor and a reference compound, which is fluorescein in 0.1 N NaOH. A_{RF} and A_D are the respective absorbances of the reference compound and donor. Q_{RF}, the quantum yield of fluorescein in 0.1 N NaOH, was taken to be 0.90 (*48*).

The efficiency of energy transfer (E) between the fluorescein and TMR probes was calculated by measuring the integrated area of the fluorescein emission peak between 500 and 515 nm, in the presence (F_{DA}) and absence (F_D) of acceptor at each position investigated. The efficiency of energy transfer is expressed by the equation

$$E = 1 - (\int F_{DA}/\int F_D) \quad (5)$$

This method of donor peak integration has been used previously to calculate transfer efficiency values (*49*).

Titration of the Fluorescein Labeled Klenow Fragment with TMR-Labeled Duplexes. A solution containing fluorescently labeled KF* (3.5 μM) in 50 mM Tris-HCl, pH 7.5, 100 mM NaCl, 0.5 mM EDTA was prepared (total volume = 80 μL). Aliquots (0.5 μL) of the fluorescent duplexes (100 μM) were added, and the steady-state fluorescence emission intensity was measured at 518 nm with excitation at 497 nm. Fluorescent template−primer was added until there was no further change in the emission intensity.

Primer Strand Extension. Primer strand extension was carried out by addition of deoxynucleoside triphosphates (dNTP's) to the solution of KF* titrated with TMR-labeled template−primers (described above). The base composition of the template strand in each of the four duplexes allows the primer to be lengthened in discrete steps by addition of appropriate dNTP's (see Figure 1). For each duplex, the initial primer extension was initiated by addition of a mixture of dTTP/dGTP (0.5 μL, 50 mM) followed by addition of $MgCl_2$ (0.4 μL, 200 mM), to initiate polymerization. A fluorescence measurement was taken after the addition of the dNTP's and another after the addition of $MgCl_2$. The fluorescence change induced by polymerization was monitored by performing scans over a period of several minutes until no further change in fluorescence intensity was observed. The next required nucleotide was added (0.25 μL, 100 mM) in order to extend the primer to the next position and the fluorescence measurements repeated. Control experiments were performed using unlabeled template−primers to account for any intrinsic quenching of fluorescein by the oligonucleotide duplexes. Complete extension of the primer strand was confirmed by DNA gel electrophoresis of ^{32}P-labeled oligonucleotides followed by visualization of bands using a Molecular Dynamics PhosphorImager.

Electrospray Mass Spectrometry of KF and Modified Oligonucleotides. The unmodified and fluorescein-modified KF were characterized by electrospray mass spectrometry using a VG-Bio Q triple quadropole mass spectrometer. Protein samples (50 μM, 20 μL) were dialyzed against 2 mM ammonium bicarbonate, 1 mM DTT using a microdialysis system (Pierce). Dialyzed samples (25 μL) were mixed with an equal volume of acetonitrile, and formic acid was added to 3% (v/v) before injection. Introduced into the ion source were 10 μL aliquots at a flow rate of 5 μL/min. The extraction cone voltage was set to 60 V and the source temperature to 70 °C. Data were acquired in the positive ion mode from m/z = 600 to m/z = 1600. Oligonucleotide samples were run as 25 μM solutions in 1:1 H_2O:2-propanol (IPA) containing 1% (v/v) triethylamine (TEA). Sodium ion contamination of oligonucleotide samples becomes critical when masses exceed 10 kDa due to the formation of oligonucleotide−sodium adducts (*50, 51*). To remove traces of sodium ion present in ESMS samples, the following purification procedure was carried out, using a modified literature method (*52*). A 1 nmol sample of oligonucleotide was dissolved in 100 μL of 5 M ammonium acetate and the sample allowed to stand at room temperature for 1 h. The oligonucleotide was precipitated by addition of 3 volumes of ice cold ethanol and placed in a methanol/dry ice bath for 2 h. The sample was recovered by centrifugation at 14000*g* for 30 min. The supernatant was removed and the sample washed with ice cold 80% ethanol. The sample was centrifuged again at 14000*g* for 20 min and the supernatant removed. This procedure was repeated, and the samples were then dissolved in the H_2O/IPA/TEA solution for ESMS analysis. Data were acquired in the negative ionization mode from m/z = 400 to m/z = 1300. All ESMS data were analyzed using MassLynx software.

Time-Resolved Fluorescence Spectroscopy. Lifetime measurements were performed on a modified inverted optical microscope (Nikon Diaphot 200). Samples were excited with a frequency doubled mode-locked solid-state Nd:YAG laser (Coherent Antares 76-s) which provided an excitation wavelength of 532 nm, a pulse width of 70 ps, and a repetition rate of 76 MHz. The laser output was attenuated by a beam splitter and coupled polarizers to less than 10 mW and passed via an objective to the sample on a coverslip. The fluorescence was collected by the same objective and separated from the excitation source by a dichroic mirror and band-pass filter (Omega Optical 540DRLP and 590DF35, respectively). Emission was detected by a fast photomultiplier (Hamamatsu R4457) with a rise time of 1.4 ns and the signal processed with a time correlated single photon

counting system (Edinburgh Instruments SPC300). An instrument response function was obtained by scattering the laser pulses from a dilute solution of microspheres, the fwhm of which was 0.5 ns. Measurements were made on independent samples of TMR modified oligonucleotides which were labeled in both the single stranded and duplex regions. Further measurements were made on the TMR modified template−primer substrates bound to nonfluorescent KF protein.

Fluorescence Lifetime Analysis. The isotropic fluorescence decay was analyzed with a multiexponential model which was convoluted with an instrument response function to give the measured lifetime curves. The measured signal is given by (*13*)

$$F(t) = I(t) \otimes D(t) \tag{6}$$

$$D(t) = \sum_{i=1}^{N} \alpha_i \exp(-t/\tau_i) \tag{7}$$

where $I(t)$ is the instrument response function, $\otimes$ denotes the convolution of two functions, α_i is the fractional amplitude associated with the component with fluorescent lifetime τ_i, and N is the number of decay components. The average fluorescent lifetime is given by

$$\tau_{av} = \sum_{i=1}^{N} \alpha_i \tau_i \tag{8}$$

The parameters α_i and τ_i are optimized for the best fit of eqs 6 and 7 to the lifetime data using a rapid Marquardt search method. The quality of fit was judged by χ_r^2, the reduced chi square parameter.

Molecular Modeling Calculations. Calculations were performed using MacroModel 4.5 adopting the Amber molecular mechanics program in the PRCG mode. Calculations were performed using water as the solvent with a convergence gradient of 0.05 kJ/Å. All hydrogens attached to carbon atoms were deleted to make calculations more rapid. Two situations were subject to energy minimizations, one with the fluorophore intercalated into the DNA base stack and the other with the fluorophore extended outside the base stack.

RESULTS

Resonance energy transfer measurements between fluorophores were used to investigate the topology of the single stranded region in a series of template−primers bound to the KF. Site-directed mutagenesis enabled production of a double mutant KF (S751C, C907S). The serine residue at position 751 in the amino acid sequence was chosen as a site of mutation as it appeared to be solvent exposed which is a necessary criterion for the covalent modification required for FRET measurements. Furthermore, this residue was in a position which was removed from the active site residues and the DNA binding cleft and therefore unlikely to interfere with the activity of the enzyme. Assuming the model proposed by Steitz and co-workers for DNA binding (*3*), residue 751 appeared suitable for use as a stationary observation point in FRET measurements. The double mutation was shown to have minimal effect on the polymerase activity as the rate of single base incorporation of dATP into a radiolabeled duplex was greater than 80% of the value obtained for the wild-type protein. Modification of this site by reaction of the free thiol with iodoacetamidofluorescein allowed its use as an energy transfer donor for the TMR acceptor fluorophore used in the template−primers. Modification was achieved by reaction of the mutant protein for 30 min at 4 °C with a 3-fold excess of fluorescent probe. When labeling was initially attempted by an overnight reaction, this resulted in multiple modification of the protein, presumably due to additional modification of lysine residues. This was observed by electrospray mass spectrometry (ESMS), which is important for the characterization of modified biomolecules, since other methods such as the Ellman titration (*53*) would not have revealed this. The labeled KF was initially identified by a second absorbance at 495 nm (fluorescein) associated with the 280 nm absorbance of the protein. Ellman titrations also indicated complete reaction. Figure 2 shows an ESMS trace of the unmodified KF protein and a second spectrogram of KF*, the single fluorescein labeled protein. The mass difference corresponds to the mass of the added fluorescein moiety (388 Da). Single base addition experiments showed that the rate of incorporation of dATP into a radiolabeled duplex by the fluorescein modified enzyme was 80% of the value obtained from the wild-type protein, indicating that the fluorescent modification did not significantly alter the activity of the enzyme.

Table 1: Calculated and Experimentally Determined Masses of TMR-Modified Oligonucleotides[a]

oligonucleotide	calcd mass (Da)	exptl mass (Da)
1	11226.2	11227.0
2	11266.2	11266.0
3	11242.2	11251.0
4	12132.9	12135.1

[a] Refer to Figure 1 for the sequences of oligonucleotides **1**−**4**.

The succinimidyl ester derivative of TMR was conjugated to either a 35 mer or 38 mer template oligonucleotide (Figure 1) containing a uridine base with a propargylamino linker at the 5-position. HPLC analysis indicated that the reactions proceeded in greater than 90% yield. The fluorescently labeled oligonucleotides were also characterized by ESMS. Figure 2c shows an ESMS trace of the modified oligonucleotide **3**, which corresponds to the expected mass increase upon conjugation with TMR. Table 1 presents the ESMS results of the four rhodamine derivatized oligonucleotides, indicating calculated and experimentally determined masses.

The fluorescently modified template oligonucleotides were annealed to the 13 mer primer strand to give fluorescent duplexes. The TMR-labeled template−primers were shown to be efficient substrates for the polymerase activity of KF*. Addition of appropriate dNTP's to ^{32}P-labeled template−primer/KF* complexes resulted in extension of the primer to the expected products (Figure 3). The binding of TMR-labeled template−primer to KF* resulted in a 2.7-fold decrease in the fluorescein emission intensity as a consequence of FRET. This decrease in emission intensity was complete upon addition of 1 equiv of template−primer, indicating the formation of a 1:1 binary complex (Figure 4).

The template in each duplex system is designed so that addition of appropriate dNTP's will extend the 13 mer primer

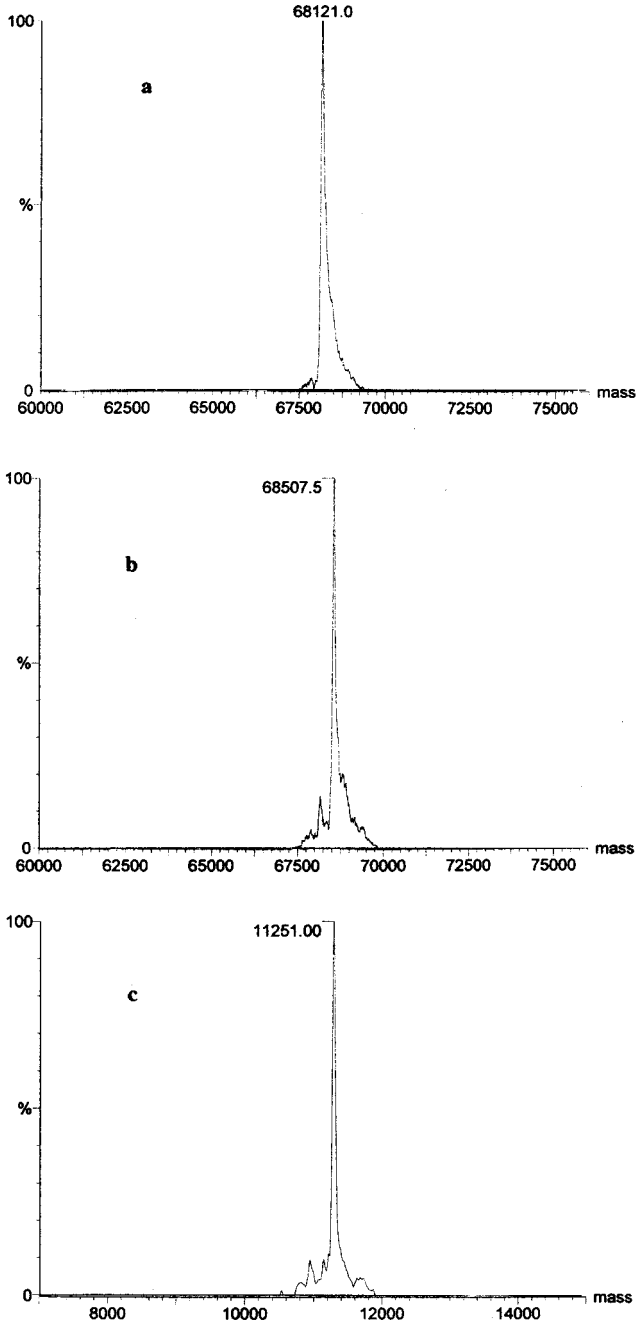

FIGURE 2: ESMS traces of (a) unmodified KF, (b) fluorescein modified KF*, and (c) TMR modified 3. The expected mass increase of the protein upon conjugation with fluorescein is 388 Da, which gives a calculated mass of 68 509 Da. This is in close agreement with the experimentally determined mass of 68 507.5 Da. The experimental mass of the TMR-modified oligonucleotide (11 251 Da) is also in close agreement with the expected mass (11 250.2 Da) after fluorescent modification.

in discrete steps. The position of the TMR probe is defined as $\pm x$ were x represents the number of nucleotides upstream (+), in the duplex region, or downstream (−), in the single stranded region, that the fluorophore is situated relative to the primer terminus (position 0; see Figure 1). In each of the four template−primer substrates, the rhodamine probe was initially at position −11 and was sequentially extended to positions −9, −6, −4, −2, +3, and +6 according to the template−primer used (Figure 1). Position −11 was chosen as a starting point for each experiment since it has been demonstrated that there are DNA−protein contacts up to this

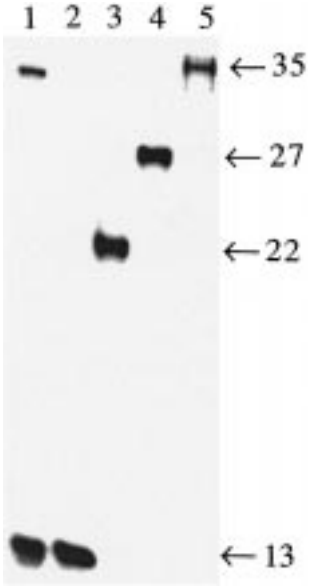

FIGURE 3: Primer strand extension of 13/35*(1) by KF*. In lane 1 both the 13 mer primer strand and 35* mer template strand were 5′-OH-labeled with ^{32}P. In lanes 2−5 only the 13 mer primer strand was ^{32}P-labeled. (Lane 1) 13/35*(1) ^{32}P-labeled standards. (Lanes 2−5) 13/35*(1) extended by addition of appropriate dNTP's: (lane 2) no dNTP's added; (lane 3) dT, dG added, resulting in extension to 22 mer product; (lane 4) dT, dG, dC added, resulting in extension to 27 mer product; (lane 5) dT, dG, dC, dA added, resulting in complete extension to 35 mer product.

Table 2: Fluorescence Parameters as a Function of TMR Position in the KF*/DNA Complexes

probe position	fluorescence intens[a,b]	transfer efficiency[b]
−11	365[c]	0.51[c]
−9	339	0.50
−6	309	0.54
−4	206	0.71
−2	195[c]	0.69[c]
+3	258	0.59
+6	198	0.70

[a] The initial fluorescence emission intensity (fluorescein) is 960. The intensity value of 365 at position −11 represents the quenching upon template−primer binding prior to initiation of polymerization. [b] The fluorescence intensity and calculated transfer efficiency at each position is the average of four independent experiments using different DNA and protein samples. [c] The fluorescence intensity and transfer efficiency at positions −11 and −2 are the average values of the four template−primer samples that initially have the probe at position −11 and of the three samples that result in extension to position −2. These values are then averaged again over the four independent experiments to give the final quoted value.

position on the template (*29*). Extension of the primer by KF* resulted in a decrease in the donor (fluorescein) emission intensity as the acceptor (TMR) probe moved through the single stranded region to position −2. This was followed by an increase in emission intensity as the probe moved into the duplex region up to position +3 and then by a further decrease as the probe moved to the +6 position (Table 2).

The initial position of the fluorophore in the four template−primers was −11, and three of the template−primers also had the fluorophore positioned at −2 at some point in the extension experiments. These points acted as internal references, as the fluorescence emission intensity values were comparable for each template−primer system, indicating they were all binding to the enzyme in the same manner. The

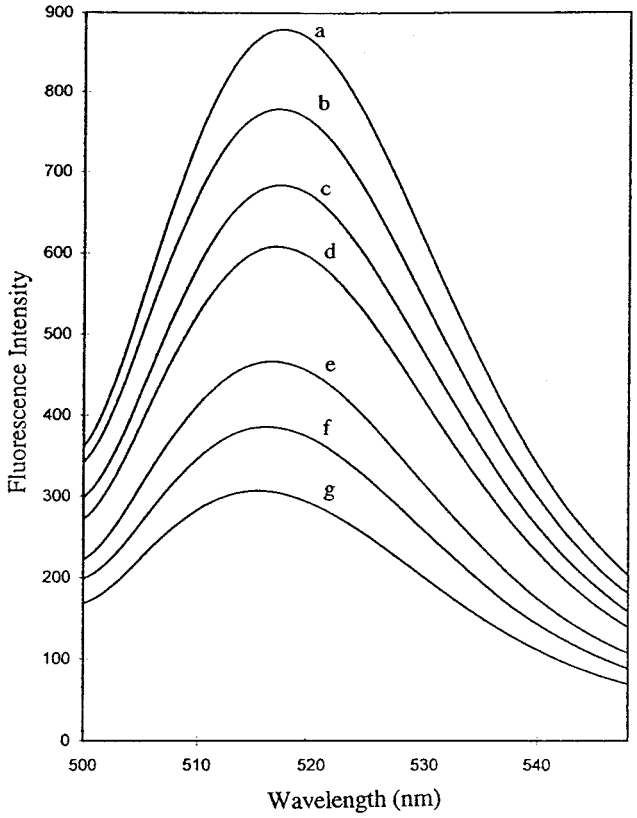

FIGURE 4: Titration of fluorescein-labeled KF* with TMR-labeled template−primer, 13/35*(1). 0.5 μL aliquots (100 mM) of DNA substrate were added to a 3.5 μM solution of KF*, and the decrease in fluorescence emission intensity was monitored. The fluorescence intensity of KF* prior to the addition of DNA substrate is shown in a. Concentrations of template−primer are (a) none (b) 0.6 μM, (c) 1.2 μM, (d) 1.8 μM, (e) 2.4 μM, (f) 3.0 μM, and (g) 3.6 μM. Final concentrations of KF* and DNA substrate are approximately 3.5 μM, after which the addition of further template−primer produces no change in the fluorescence intensity, indicating the formation of a 1:1 complex.

efficiency of energy transfer (E) between the fluorescent probes was calculated for each of the seven positions in the duplex using eq 5. These efficiencies as well as the fluorescence intensity values for each position are presented in Table 2. The efficiency of energy transfer as a function of probe position is shown by the data points in Figure 5. The line in this figure represents the results of the simulation which is described in the Discussion.

These findings demonstrate intramolecular energy transfer between the fluorescein donor and the TMR acceptor. The efficiency of energy transfer was in the range of 50−71% (Table 2). The quantum yield of the donor in the absence of acceptor, Q_D, was determined to be 0.55. The overlap integral between the donor and acceptor, J_{DA}, was 3.86 × 10^{-13} M^{-1} cm^3, and the Forster critical distance, R_0, was determined to be 58.5 Å. This R_0 value is in good agreement with previously reported values for the fluorescein donor/TMR acceptor pair (*54*).

Control experiments involving binding and extension of unlabeled template−primer substrates by KF* showed no significant quenching of the fluorescein probe, indicating that all observed changes in fluorescence intensity were a consequence of FRET between the donor and acceptor fluorophores.

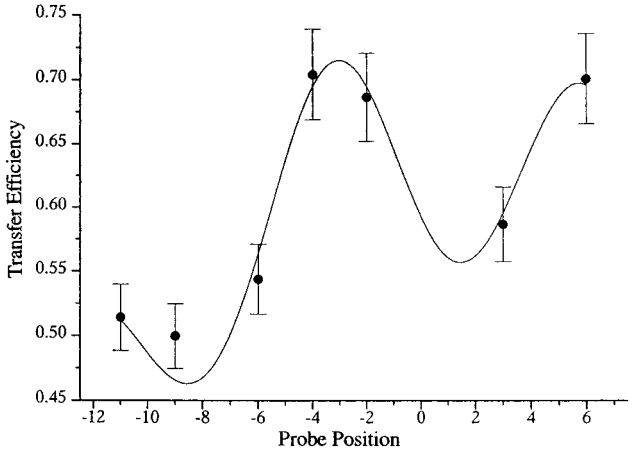

FIGURE 5: Experimental FRET efficiencies as a function of probe position (circles) and simulation (line) using a simple vector model of the DNA−polymerase interaction (see Figure 7). Each data point is an average of four independent experiments. Further details are described in footnotes *b* and *c* to Table 2. Error bars represent a maximum error of 6%.

Fluorescence Lifetime Results. Time-resolved fluorescence spectroscopy is a powerful technique capable of probing the structural and dynamic features of macromolecules and supramolecular assemblies such as proteins and nucleic acids (*55*). One of the principal parameters that can be measured using time-resolved techniques is the orientation and movement of a chromophore relative to the framework of a system of biological interest. The fluorescent lifetime depends on the properties of the molecular environment of the fluorescent probe. Thus, any particular environment or changes therein may be probed by its influence on the fluorescence decay kinetics (*55*).

Time-resolved measurements were performed in order to provide information regarding the orientation of the fluorescent TMR probe attached to the DNA substrates. The fluorescence lifetime experiments used two separate 13/35 mer duplexes with the TMR fluorescent probe covalently attached to the 13 mer and 35 mer, respectively. The sequences of the duplexes and positions of the TMR probe (indicated by U*) are given as follows:

sequence 1: 3′-AGCGTCGGCAGGTACCACAA
CATTCACGAGGCATG-5′

5′-TCGCAGCCG**U***CCA

sequence 2: 3′-AGCGTCGGCAGGTACCACGA
CAT**U***CACGAGGCATG-5′

5′-TCGCAGCCGTCCA

This allowed comparison of the lifetime of the TMR probe for samples in which the probe was attached to a base that was part of a helical structure sequence 1 and in which the probe resided in the single stranded region sequence 2, as in the FRET experiments.

The optimized lifetimes of the two template−primer samples, both in solution and bound to nonfluorescent KF protein, are presented in Table 3 along with the relative amplitudes and the reduced χ^2 indicators.

TMR-modified oligonucleotides both in solution and bound to nonfluorescent KF protein require a biexponential

Table 3: Fluorescent Lifetimes of TMR-Labeled Template−Primer[a]

	TMR-labeled 13/35* duplex			
	(a)	bound to KF (a)	(b)	bound to KF (b)
	Two Component			
τ_1 (ns)	3.64 ± 0.32	3.56 ± 0.28	3.61 ± 0.39	3.47 ± 0.42
α_1	0.81 ± 0.03	0.63 ± 0.08	0.82 ± 0.09	0.58 ± 0.14
τ_2 (ns)	0.76 ± 0.11	0.94 ± 0.06	1.61 ± 0.51	1.39 ± 0.09
α_2	0.19 ± 0.03	0.37 ± 0.03	0.18 ± 0.11	0.42 ± 0.05
τ_{av} (ns)	3.09 ± 0.11	2.39 ± 0.09	3.25 ± 0.30	2.38 ± 0.21
χ_r^2	1.06	1.09	1.05	1.04
	One Component			
τ (ns)	2.32 ± 0.06	1.82 ± 0.15	2.88 ± 0.08	1.93 ± 0.14
χ_r^2	1.34	1.46	1.12	1.42

[a] Optimized parameters obtained from the fitting of a biexponential and a single component decay to the fluorescence lifetime measurements of the acceptor TMR in (a) conjugated to the template strand in a 13/35* template−primer system in the absence and presence of nonfluorescent KF protein and (b) conjugated to the primer strand in a 13*/35 duplex in the absence and presence of nonfluorescent KF protein. τ_1, τ_2, and τ_{av} are the fluorescent lifetimes in nanoseconds. α_1 and α_2 are the fractional amplitudes associated with each fluorescent lifetime. The quality of fit is judged by χ_r^2, the reduced chi square parameter.

Table 4: Fluorescence Anisotropy Values for Fluorescein-Labeled KF* and TMR-Labeled Duplexes[a]

fluorescent component	anisotropy	fluorescent component	anisotropy
KF*	0.1064	KF:13*/35[c]	0.1541
KF*:13/35[b]	0.0829	13/35*[d]	0.1050
13*/35[c]	0.0923	KF:13/35*[d]	0.1725

[a] Anisotropy measurements were performed on KF* in solution and bound to a nonfluorescent duplex, as well as TMR-labeled duplexes in solution and bound to nonfluorescent KF protein. [b] 13/35 refers to the nonfluorescent duplex. [c] 13*/35 refers to the fluorescent duplex where the TMR probe is attached to the 13 mer primer strand in the duplex region. [d] 13/35* refers to the fluorescent duplex where the TMR probe is attached to the 35 mer template strand in the single stranded region.

decay to provide a sufficiently accurate fit to the lifetime data, as indicated from the lower χ_r^2 value for a two component fit compared to that of a one component fit. The contribution of both long- and short-lived components to the fluorescent lifetime of the modified substrates is indicative of heterogeneity in the environment of the fluorescent label. The preexponential factors (α_1 and α_2) for each lifetime component are proportional to the relative population of each species (*14*), which suggests a greater tendency for the dye molecule to exist in a state which interacts with the DNA, possibly through intercalation. The bearing these results may have on the proposed helical model are described further in the Discussion.

Anisotropy Results. The anisotropy of the fluorescein and TMR fluorophores, indicative of the freedom of rotation, was also measured for the fluorescently labeled protein and template−primers. The sequence of the 13/35 mer duplex and the position of the TMR probe was the same as that used for the fluorescence lifetime measurements. Anisotropy values were obtained for the individual fluorescent protein and template−primer components and for the protein−nucleic acid complexes (Table 4).

Molecular Modeling Results. Molecular modeling calculations were performed in order to determine the possibility of intercalation of the TMR fluorophore within the DNA base stack. Energy minimizations were performed on two duplex samples, one with the fluorophore extended outside the base stack and exposed to the solvent and another with the fluorophore intercalated into the DNA base stack. The energies of the minimized structures were calculated to be −23 410 kJ/mol for the extended form and −23 433 kJ/mol for the intercalated form.

DISCUSSION

Direct observation of the structure and conformation of the single stranded template region of DNA substrates bound to the KF, or any DNA polymerase, has been hindered by the apparent difficulty in obtaining cocrystal structures of the polymerase−DNA complexes (*4*). Although there have been a number of crystal structures of KF with complexed DNA (*3*, *5*), none have shown a competent complex with the 3′-terminus situated at the polymerase active site and containing a 5′ template overhang interacting with the enzyme. All DNA polymerases characterized to date have many structural and functional similarities. This then raises the question of whether they also bind their DNA substrates in a similar manner and if the ordered structure of a template−primer bound to one polymerase may apply to other polymerases.

The possibility of the existence of an ordered structure in the single stranded template region of DNA substrates bound to the KF was first suggested by Benkovic and co-workers (*29*). This investigation addressed protein−DNA interactions in the single stranded region of a template−primer system. On the basis of observed changes in the fluorescence emission intensity and fluorescence anisotropy of the fluorophore as it occupied different positions in the single stranded region, it was suggested that the template strand may adopt a helical conformation when bound to the enzyme, but this hypothesis was never thoroughly investigated.

In the present study, we have utilized the technique of FRET to investigate the structure of the single stranded template in a series of DNA substrates bound to the KF. Figure 6 depicts a schematic illustration of the established mode of DNA binding (*3*, *22*) and illustrates the relative positions of the donor and acceptor fluorophores. Chemical footprinting (*56*), fluorescence (*13*, *29*), and photo-cross-linking (*57*) experiments together indicate that 5−8 base pairs of duplex DNA are covered by the KF when the primer terminus is at the polymerase site (*58*). Furthermore, DNA−protein contacts have been shown to exist up to 11 bases downstream in the single stranded template region (*29*).

Figure 5 shows a plot of the efficiency of energy transfer (*E*) between the fluorescein donor probe on the protein and the TMR acceptor at various positions in the single stranded and duplex regions. The distribution of data points suggest the existence of some ordered structure in the single stranded region. The oscillation in the data points would appear to rule out the possibility of a linear conformation of the single stranded template. Rather, the modulation of the data suggests a helical conformation of the single stranded template bound to the enzyme. To test this hypothesis, a simple mathematical model (Figure 7 and eq 9) was formulated to correlate the fluorescence data with helical structure. The model describes a helical structure with little or no

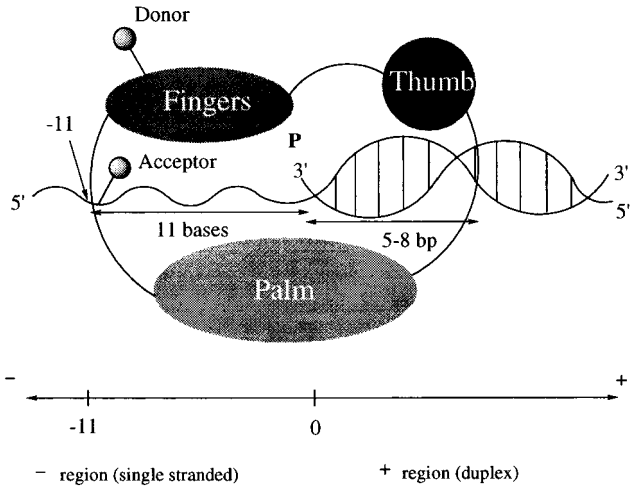

FIGURE 6: Schematic diagram of template−primer substrate bound to the KF indicating the relative positions of the donor and acceptor fluorophores and the numbering system used. The 3′-OH at the primer terminus (P) is defined as position 0 and each base given a numerical value based on the distance from the primer−terminus, with bases in the duplex and single stranded regions given positive and negative values, respectively.

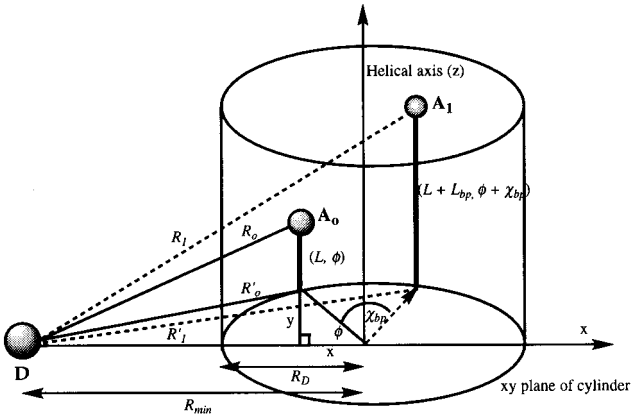

FIGURE 7: Schematic representing helical movement of the TMR fluorophore through the single stranded region and into the duplex region of the DNA molecule. ϕ represents the cylindrical angle between D and A in the *xy* plane (perpendicular to the helical axis) when $N = 0$. L represents the theoretical vectorial distance between A and the projection onto the *xy* plane when $N = 0$ (L can be negative). χ_{bp} and L_{bp} represent the angular rotation and linear displacement per base pair added. L_{bp} is subject to error as explained by the fact that the projection of the molecular center of the acceptor on the helical axis does not necessarily correspond to the plane of the base unit to which it is attached (*35*). R_D represents the radius of the helix and R_{min} the perpendicular distance between the DNA axis and the donor fluorophore. Position A_0 represents the theoretical starting point of the acceptor fluorophore relative to the donor, and position A_1 represents the theoretical position of the same fluorophore after the addition of one base pair ($N = 1$). Vectors R_0 and R_1 originate on the donor molecule and point toward the acceptor molecules A_0 and A_1, respectively. R' is the component of R projected onto the *xy* plane.

degree of flexibility. Clegg and co-workers have applied a similar treatment to model FRET data to confirm the structure of duplex DNA (*35*). In our analysis of the FRET data, we have assumed that the orientation factor (κ^2) has a value of $^2/_3$. This would correspond to a rapid randomization of the relative orientation of the donor and acceptor dipoles, which has generally been assumed in similar studies (for examples see refs 34, 35, and 47). Anisotropy values of the fluorescently labeled protein and template−primer substrates were measured to be less than 0.2 (Table 4), which suggests that the assumption that $\kappa^2 = {}^2/_3$ is reasonable (*30*).

This model defines the cylindrical geometry of the DNA helix and the vectorial distance between the donor and acceptor fluorophores. A description of the parameters used in the model is as follows. D represents the donor fluorescein fluorophore which maintains a stationary position on the protein. A_0 defines the initial position of the acceptor TMR fluorophore prior to the addition of the next base in the sequence. The parameters L and ϕ represent this initial position of the TMR probe, where L is the vectorial distance between A_0 and its projection onto the *xy* plane (which is perpendicular to the helical axis and in the same plane as the donor fluorophore) and ϕ represents the initial cylindrical angle between D and A_0. The model describes the movement of the TMR probe from position A_0 to A_1 upon addition of a single base pair. Two new parameters, L_{bp} and χ_{bp}, define the new probe position. It is these two parameters, along with R_D, that are most significant to the model as they define the physical structure of the helix. R_D represents the radius of the helix and L_{bp} and χ_{bp} define the linear displacement and angular rotation per base pair added.

There are a number of examples of single stranded nucleic acids with helical structure (*59*). Circular dichroism (*60*) and optical rotatory dispersion (ORD) (*61*) studies indicate that the homopolymer poly(ribocytidylic acid), poly(C), occurs in a helical configuration in aqueous solution at neutral pH. X-ray fiber diffraction studies of poly(C) (*62*) and poly(2′-O-methyl-C) (*63*) have shown the existence of a right-handed, single stranded helix containing six bases per pitch of 18.6 and 18.9 Å, respectively. The rise per base pair (L_{bp}) is 3.1 Å for poly(C) and 3.2 Å for poly(2′-O-methyl-C) and the angular rotation per base pair (χ_{bp}) is 60°. The radius of the helix (R_D) was not available. Subsequent NMR studies of poly(C) in neutral solution support the existence of a novel left-handed helical structure (*64*). Solution studies of polyriboadenylic acid, poly(A), also indicate the existence of a helical structure at neutral pH (*65*). Mathematical derivation of an extended conformation from the crystal structure of a poly(A) fragment (*66*) produces a single stranded helix containing nine nucleotides per pitch of 25.4 Å, with values of 2.8 Å for L_{bp}, 40° for χ_{bp}, and a helical radius (R_D) of 10.7 Å (*67*). The parameters L_{bp}, χ_{bp}, and R_D also bear relation to the known structure of duplex DNA. The physical characteristics of double helical B-form DNA are defined by the fact that a complete turn of the helix is 36 Å in length and contains approximately 10 base pairs of DNA. The rise per base pair (L_{bp}) is 3.3 Å, the angular rotation per base pair (χ_{bp}) is 36°, and the helical radius (R_D) is approximately 12 Å.

In the structural model, the magnitude of the donor−acceptor separation R is defined by the linear displacement of the acceptor along the axis of the DNA helix and the component perpendicular to the helical axis which varies sinusoidally. The vector addition of these components gives an expression for the magnitude of R to be

$$R^2 = [R_{min} - R_D\cos(\phi + N\chi_{bp})]^2 + [R_D \sin(\phi + N\chi_{bp})]^2 + (L + NL_{bp})^2 \quad (9)$$

It is clear that R varies nonlinearly with the translocation

Table 5: FRET Simulation Parameters[a]

param	simulation	poly(C)[b]	poly(A)[c]	B-form DNA[d]	A-form DNA[d]	Z-form DNA[d]
R_0 (Å)	58.5 (fixed)			–	–	–
R_{min} (Å)	52.86 ± 0.68			–	–	–
L (Å)	-0.88 ± 1.05			–	–	–
ϕ (Å)	127.2 ± 11.8					
R_D (Å)	3.78 ± 0.58	*e*	10.7	11.8	12.7	9.0
χ_{bp} (deg)	39.3 ± 2.3	60	40	36	33.6	−30
L_{bp} (Å)	2.31 ± 0.31	3.1	2.8	3.3	2.3	3.8

[a] Optimized parameters obtained from the simulation of FRET efficiencies using the simple vector model of the DNA−polymerase interaction (see text, Figure 7), and expected values defining the geometry of the homopolymer helixes, poly(C) and poly(A) and A-, B-, and Z-form duplex DNA for comparison. [b] Data obtained from ref 61. [c] Data obtained from ref 62. [d] Data obtained from ref 68 and references cited therein. [e] Data unavailable.

(NL_{bp}) and rotation ($N\chi_{bp}$) of the DNA through the polymerase and that this nonlinearity gives rise to the characteristic modulation in the FRET efficiencies (Figure 5) as defined by Förster transfer theory (eqs 1−3).

These experiments investigated a series of four template−primer substrates (Figure 1) whose sequences enabled the TMR fluorophore to occupy seven different positions: −11, −9, −6, −4, and −2 in the single stranded region as well as +3 and +6 in the duplex region. The efficiency of energy transfer at each position was calculated on the basis of the integrated areas of the fluorescein emission in the presence and absence of acceptor TMR (eq 5, Table 2). Equation 9 was used to simulate the calculated transfer efficiencies. The result of the simulation is presented in Figure 5. The parameters R_{min}, ϕ, L, R_D, L_{bp}, and χ_{bp} were optimized according to a nonlinear least-squares fitting of eq 9 to the transfer efficiency data. While previously measured values of R_0 (the characteristic distance for a donor−acceptor pair at which $E = 50\%$) vary between 40 and 60 Å, our experimentally determined value of 58.5 Å was used in the simulation. The results of the optimization are presented in Table 5 along with the values that define the geometry of the single stranded helixes, poly(A) and poly(C), as well as A, B, and Z-form duplex DNA for comparison.

Interestingly, the simulation value for χ_{bp} of 39.3° is close to the value of 40° for the poly(A) single stranded helix. Furthermore, the simulated value for L_{bp} of 2.3 Å is also close to the value of 2.8 Å for the poly(A) structure. This suggests that the structure of the template strand in a duplex substrate bound to the KF is similar to the helical structure of poly(A) in solution. The value for χ_{bp} of 39.3° obtained from the simulation is also similar to the value of 36° for B-form duplex DNA. The simulated value for L_{bp} of 2.3 Å is the same as the value for A-form duplex DNA (cf. 3.3 Å for B-form duplex DNA). The crystal structures of polymerase-bound duplex DNA substrates show characteristics of both A- and B-form DNA (*22*).

The sinusoidal oscillation of the transfer efficiency (Figure 5) is indicative of an ordered helical structure with a period of approximately 10 bases. This compares well with the 9 base periodicity of the poly(A) single helix, as well as the double helical structures of both A- and B-form duplex DNA. The simulated value of the helix radius (R_D) of 3.8 Å is small in comparison to the values for the poly(A) helix (10.7 Å) and for A- and B-form duplex DNA (12.7 and 11.8 Å, respectively). However, this simulated value of R_D may not faithfully represent the distance from the helical axis to the outer edge of the helix, since it actually depends upon the distance from the helical axis to the center of the TMR fluorophore. Since the TMR probe is attached to the template strand via a flexible linker (Figure 1), it can potentially adopt a variety of conformations ranging from being fully extended away from the helical structure to being positioned within the DNA structure with possible intercalation. Model studies were carried out on duplex DNA, labeled with TMR in the *double stranded* region to explore possible conformations. Molecular modeling calculations showed that the TMR fluorophore could fold back and intercalate between the DNA bases without significant perturbation of the structure. The difference in energy between the minimized structures in which the TMR fluorophore was either intercalated within the base stack or extended outside the base stack was small (0.1% of the total energy). Distance measurements for the intercalated minimized structure indicated that the center of the fluorophore was approximately 3.5 Å from the helical axis. If this structure reflects the TMR conformation in the FRET studies, then the value of 3.8 Å for R_D obtained could be representative of a larger helix diameter.

Time-resolved fluorescence techniques can distinguish between environments based on the fluorescence lifetime of the probe. Fluorescence lifetime studies by Vamosi et al. (*68*) concluded that, in a 5′-rhodamine-modified oligonucleotide in single stranded or duplex form, there are a number of conformations in which the dye molecule is interacting with the DNA. Previous studies using the dansyl fluorescent probe have shown that the fluorescence quantum yield and fluorescence lifetimes increase when the dansyl group is located in a hydrophobic environment (*13*). The fluorescent decays obtained for TMR attached to the double and single stranded regions of a template−primer duplex, in the absence and presence of nonfluorescent KF protein, exhibited biexponential behavior corresponding to two distinct environments, with fluorescent lifetimes similar to those observed by Vamosi et al. (*68*) (Table 3). The slower component (τ_1), which arises from some degree of internalization of the dye molecule in the template−primer structure (*13*), was the more populated. This suggests that the probe may be positioned in a hydrophobic environment between the DNA bases, in accord with the predictions based on molecular modeling. It is therefore possible that, in the FRET experiments, the TMR probe may in fact be located within the proposed helix, resulting in a reduced value of R_D for the simulation.

In conclusion, we have explored the structure of the single stranded region of a series of template−primers when bound to the KF. We propose that the single stranded 5′ template overhang is ordered and may adopt a helical conformation. It remains to be determined whether an ordered template conformation is a common structural feature of all DNA polymerases and whether the conformation has functional significance. Our results further support FRET as a useful method for the exploration of structure and conformation in protein−DNA complexes.

ACKNOWLEDGMENT

We thank Steven J. Benkovic for helpful discussions, Imogen Horsey for help with molecular modeling, Xiaojun

Chen Sun for help with mutagenesis, and Joe Jaeger for helpful discussions.

NOTE ADDED IN PROOF

After this paper had been accepted, two recent publications have appeared featuring polymerase-nucleic acid cocrystal structures for the T7 [Doublie et al. (1998) *Nature 391*, 251−258] and *Bacillus* [Kiefer, J. R. (1998) *Nature 391*, 304−307] polymerases.

REFERENCES

1. Kornberg, A. (1980) *DNA Replication*, Freeman, San Francisco.
2. Ollis, D. L., Brick, P., Hamlin, R., Xuong, N. G., and Steitz, T. A. (1985) *Nature 313*, 762−766.
3. Beese, L. S., Derbyshire, V., and Steitz, T. A. (1993) *Science 260*, 352−355.
4. Beese, L. S., Friedman, J. M., and Steitz, T. A. (1993) *Biochemistry 32*, 14095−14101.
5. Freemont, P. S., Friedman, J. M., Beese, L. S., Sanderson, M. R., and Steitz, T. A. (1988) *Proc. Natl. Acad. Sci. U.S.A. 85*, 8924−8928.
6. Dahlberg, M. E., and Benkovic, S. J. (1991) *Biochemistry 30*, 4835−4843.
7. Kuchta, R. D., Mizrahi, V., Benkovic, P. A., Johnson, K. A., and Benkovic, S. J. (1987) *Biochemistry 26*, 8410−8417.
8. Kuchta, R. D., Benkovic, P., and Benkovic, S. J. (1988) *Biochemistry 27*, 6716−6725.
9. Derbyshire, V., Freemont, P. S., Sanderson, M. R., Beese, L., Friedman, J. M., Joyce, C. M., and Steitz, T. A. (1988) *Science 240*, 199−201.
10. Derbyshire, V., Grindley, N. D. F., and Joyce, C. M. (1991) *Embo J. 10*, 17−24.
11. Polesky, A. H., Steitz, T. A., Grindley, N. D. F., and Joyce, C. M. (1990) *J. Biol. Chem. 265*, 14579−14591.
12. Polesky, A. H., Dahlberg, M. E., Benkovic, S. J., Grindley, N. D. F., and Joyce, C. M. (1992) *J. Biol. Chem. 267*, 8417−8428.
13. Guest, C. R., Hochstrasser, R. A., Dupuy, C. G., Allen, D. J., Benkovic, S. J., and Millar, D. P. (1991) *Biochemistry 30*, 8759−8770.
14. Hochstrasser, R. A., Carver, T. E., Sowers, L. C., and Millar, D. P. (1994) *Biochemistry 33*, 11971−11979.
15. Jacobo-Molina, A., Ding, J. P., Nanni, R. G., Clark, A. D., Lu, X. D., Tantillo, C., Williams, R. L., Kamer, G., Ferris, A. L., Clark, P., Hizi, A., Hughes, S. H., and Arnold, E. (1993) *Proc. Natl. Acad. Sci. U.S.A. 90*, 6320−6324.
16. Kohlstaedt, L. A., Wang, J., Friedman, J. M., Rice, P. A., and Steitz, T. A. (1992) *Science 256*, 1783−1790.
17. Arnold, E., Jacobo-Molina, A., Nanni, R. G., Williams, R. L., Lu, X., Ding, J., Clark, A. D., Zhang, A., Ferris, A. L., Clark, P., Hizi, A., and Hughes, S. H. (1992) *Nature 357*, 85−89.
18. Georgiadis, M. M., Jessen, S. M., Ogata, C. M., Telesnitsky, A., Goff, S. P., and Hendrickson, W. A. (1995) *Structure 3*, 879−892.
19. Sousa, R., Chung, Y. J., Rose, J. P., and Wang, B. C. (1993) *Nature 364*, 593−599.
20. Davies, J. F., Almassy, R. J., Hostomska, Z., Ferre, R. A., and Hostomsky, Z. (1994) *Cell 76*, 1123−1133.
21. Pelletier, H., Sawaya, M. R., Kumar, A., Wilson, S. H., and Kraut, J. (1994) *Science 264*, 1891−1903.
22. Eom, S. H., Wang, J. M., and Steitz, T. A. (1996) *Nature 382*, 278−281.
23. Kim, Y., Eom, S. H., Wang, J., Lee, D. S., Suh, S. W., and Steitz, T. A. (1995) *Nature 376*, 612−616.
24. Korolev, S., Nayal, M., Barnes, W. M., Di Cera, E., and Waksman, G. (1995) *Proc. Natl. Acad. Sci. U.S.A. 92*, 9264−9268.
25. Beese, L. S., Kiefer, J. R., Mao, C., Hansen, C. J., Basehore, S. L., Hogrefe, H. H., and Braman, J. C. (1997) *Structure 5*, 95−108.
26. Pelletier, H. (1994) *Science 266*, 2025−2026.
27. Sawaya, M. R., Pelletier, H., Kumar, A., Wilson, S. H., and Kraut, J. (1994) *Science 264*, 1930−1935.
28. Steitz, T. A., Smerdon, S. J., Jager, J., and Joyce, C. M. (1994) *Science 266*, 2022−2025.
29. Allen, D. J., Darke, P. L., and Benkovic, S. J. (1989) *Biochemistry 28*, 4601−4607.
30. Clegg, R. M. (1992) *Methods Enzymol. 211*, 353−388.
31. Selvin, P. R. (1995) *Methods Enzymol. 246*, 300−334.
32. Wu, P. G., and Brand, L. (1994) *Anal. Biochem. 218*, 1−13.
33. Miki, M., and Kouyama, T. (1994) *Biochemistry 33*, 10171−10177.
34. Allen, D. J., and Benkovic, S. J. (1989) *Biochemistry 28*, 9586−9593.
35. Clegg, R. M., Murchie, A. I. H., Zechel, A., and Lilley, D. M. J. (1993) *Proc. Natl. Acad. Sci. U.S.A. 90*, 2994−2998.
36. Parkhurst, K. M., and Parkhurst, L. J. (1995) *Biochemistry 34*, 285−292.
37. Yang, M. S., Ghosh, S. S., and Millar, D. P. (1994) *Biochemistry 33*, 15329−15337.
38. Joyce, C. M., and Derbyshire, V. (1995) *Methods Enzymol. 262*, 3−13.
39. Joyce, C. M., and Grindley, N. D. F. (1983) *Proc. Natl. Acad. Sci. U.S.A. 80*, 1830−1834.
40. Setlow, P., Brutlag, B., and Kornberg, A. (1972) *J. Biol. Chem. 247*, 224−228.
41. Ozaki, H., and McLaughlin, L. W. (1992) *Nucleic Acids Res. 20*, 5205−5214.
42. Sambrook, J., Fritsch, E. F., and Maniatis, T. (1989) *Molecular Cloning, A Laboratory Manual*, 2nd ed., Cold Spring Harbor Laboratory Press, Plainview, NY.
43. Lackowicz, J. R. (1983) *Principles of Fluorescence Spectroscopy*, Plenum Press: New York.
44. Wu, C. W., and Stryer, L. (1972) *Proc. Natl. Acad. Sci. U.S.A. 69*, 1104−1108.
45. Stryer, L., and Haughland, R. P. (1967) *Proc. Natl. Acad. Sci. U.S.A. 58*, 719−726.
46. Fairclough, R. H., and Cantor, C. R. (1978) *Methods Enzymol. 48*, 347−379.
47. Chapman, E. R., Alexander, K., Vorherr, T., E., C., and Storm, D. R. (1992) *Biochemistry 31*, 12819−12825.
48. Demas, J. N., and Crosby, G. A. (1971) *J. Phys. Chem. 75*, 991−1024.
49. Isaac, V. E., Patel, L., Curran, T., and Abateshen, C. (1995) *Biochemistry 34*, 15276−15281.
50. Bleicher, K., and Bayer, E. (1994) *Biol. Mass Spectrom. 23*, 320−322.
51. Smith, R. D., Loo, J. A., Edmonds, C. G., Barinaga, C. J., and Udseth, H. R. (1990) *Anal. Chem. 62*, 882−889.
52. Potier, N., Van Dorsselaer, A., Cordier, Y., Roch, O., and Bischoff, R. (1994) *Nucleic Acids Res. 22*, 3895−3903.
53. Ellman, G. L. (1958) *Arch. Biochem. Biophys. 74*, 443−449.
54. Eis, P. S., and Millar, D. P. (1993) *Biochemistry 32*, 13852−13860.
55. Holzwarth, A. R. (1995) *Methods Enzymol. 246*, 334−361.
56. Joyce, C. M., and Steitz, T. A. (1987) *Trends Biochem. Sci. 12*, 288−292.
57. Catalano, C. E., Allen, D. J., and Benkovic, S. J. (1990) *Biochemistry 29*, 3612−3621.
58. Joyce, C. M., and Steitz, T. A. (1994) *Annu. Rev. Biochem. 63*, 777−822.
59. Saenger, W. (1983) in *Principles of Nucleic Acid Structure* (Cantor, C. R., Ed.) pp 298−320, Springer-Verlag, New York.
60. Brahms, J. (1967) *J. Am. Chem. Soc. 85*, 3298.
61. Fasman, G. D., Lindblow, C., and Grossman, L. (1964) *Biochemistry 3*, 1015−1021.
62. Arnott, S., Chandrasekharan, R., and Leslie, A. G. W. (1976) *J. Mol. Biol. 106*, 735−738.
63. Leslie, A. G. W., and Arnott, S. (1978) *J. Mol. Biol. 119*, 399−414.
64. Broido, M. S., and Kearns, D. R. (1982) *J. Am. Chem. Soc. 104*, 5207−5216.

65. Scovell, W. M. (1978) *Biopolymers 17*, 969−984.
66. Suck, D., Manor, P. C., Germain, G., Schwalbe, C. H., Weimann, G., and Saenger, W. (1973) *Nature New Biol. 246*, 161−164.
67. Saenger, W., Riecke, J., and Suck, D. (1975) *J. Mol. Biol. 93*, 529−534.
68. Vamosi, G., Gohlke, C., and Clegg, R. M. (1996) *Biophys. J. 71*, 972−994.
69. Dickerson, R. E., Drew, H. R., Conner, B. N., Wing, R. N., Fratini, A. V., and Kopka, M. L. (1982) *Science 216*, 475−485.

BI9719758